ACS Partner Journal

ACCOUNTS
—of materials research—

pubs.acs.org/amrcda

Article

# Framing Silver Nanocrystals with a Second Metal to Enhance Shape Stability and Expand Functionality

Dong Qin*

Cite This: *Acc. Mater. Res.* 2022, 3, 391−402

Read Online

ACCESS | Metrics & More | Article Recommendations

**CONSPECTUS:** Silver nanocrystals embrace fascinating properties for a wide variety of applications, but their performance tends to deteriorate because of shape instability arising from the dissolution of Ag atoms from high-energy sites such as edges and vertices. This issue can be addressed by framing the particle with a more stable metal M for the generation of a Ag@M core-frame nanocrystal. In addition to the improvement in shape stability, the inclusion of metal M expands the functionality and capability of the Ag nanocrystals. The first part of this Account introduces two strategies for the rational synthesis of Ag-based core-frame nanocubes. In the first strategy, a precursor to metal M is cotitrated with $Ag^+$ ions into an aqueous suspension of Ag nanocubes in the presence of ascorbic acid ($H_2Asc$, reducing agent) and poly(vinylpyrrolidone) (PVP, colloidal stabilizer) under ambient conditions. The M and Ag atoms derived from the two precursors are preferentially codeposited along the edges of Ag nanocubes for the creation of Ag@M-Ag core-frame nanocubes. The second strategy combines the carving of Ag from the side faces of Ag nanocubes and the concurrent deposition of M and Ag atoms on the edges in an orthogonal fashion. In one protocol, the precursor to M is titrated into an aqueous suspension of Ag nanocubes in the presence of $H_2Asc$, sodium hydroxide (pH modifier), and cetyltrimethylammonium chloride (colloidal stabilizer and surface capping agent) under ambient conditions. In another protocol, the precursor is titrated into a mixture of Ag nanocubes, PVP (colloidal stabilizer and surface capping agent), and ethylene glycol (solvent and reducing agent) at an elevated temperature. In both cases, Ag atoms are carved from the side faces via oxidative etching while M and Ag atoms derived from the chemical reduction are codeposited on the edges for the generation of Ag@M-Ag core-frame concave nanocubes. The second part of this Account showcases the augmented properties of the Ag-based core-frame nanocrystals, in addition to some new functionality. The first example demonstrates how to preserve the shape of Ag nanocubes at an elevated temperature by passivating the vulnerable edges with Ir frames. The second example highlights the use of Ag−Pd core-frame nanocubes as a SERS probe for in situ monitoring the Pd-catalyzed reduction of 4-nitrothiophenol to 4-aminothiophenol by $NaBH_4$ and the subsequent Ag-catalyzed oxidation of 4-ATP to *trans*-4,4′-dimercaptoazobezene by the oxygen from air. The third example establishes a method for the transformation of Ag@Au−Au core-frame concave nanocubes into trimetallic cage cubes through a site-selective galvanic replacement reaction. Altogether, these studies demonstrate that the shape stability of Ag nanocrystals can be enhanced while introducing new functionality by framing their edges with a different metal.

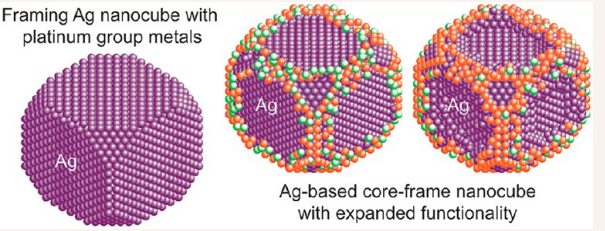




## 1. INTRODUCTION

Silver nanocrystals have received ever-increasing attention for their use in plasmonics,[1] optical detection,[2] and catalysis.[3] It is well-established that the geometric shape of a Ag nanocrystal plays an important role in controlling its properties and thereby determining its performance in various applications. For example, the shape of a Ag nanocrystal defines the number of modes allowed for localized surface plasmon resonance (LSPR).[4] The shape also controls sharp features such as edges and corners on the surface and thus the distribution of local electric fields that are essential to surface-enhanced Raman scattering (SERS).[5] However, it has been a challenge to preserve the different shapes reported for Ag nanocrystals because most of them are kinetic products. It is well documented that Ag is vulnerable to oxidative etching and thus dissolution in an environment that involves oxidants, halides, acids, and/or heating.[6,7] When Ag nanocubes were aged in a polyol at an elevated temperature, for example, their sharp edges and vertices would be quickly truncated to take a rounded profile.[7] Such a change in shape would deteriorate the SERS activity of Ag nanocubes due to the elimination of sharp features beneficial to the enhancement of local electric fields.[6] It would also increase the proportion of {111} facets on the surface, compromising the

**Received:** December 8, 2021
**Revised:** January 19, 2022
**Published:** February 3, 2022

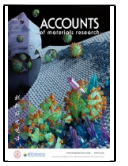





https://doi.org/10.1021/accountsmr.1c00269
*Acc. Mater. Res.* 2022, 3, 391−402

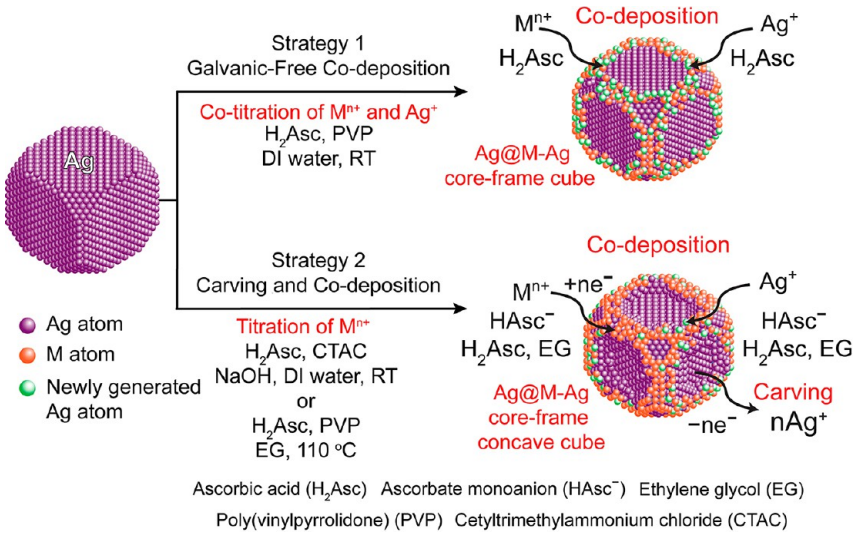


**Figure 1.** Schematic illustration showing two strategies for transforming a Ag nanocube into a Ag@M-Ag core-frame nanocube and a Ag@M-Ag core-frame concave nanocube, respectively. Modified with permission from ref 28. Copyright 2018 American Chemical Society.

selectivity of Ag nanocubes as a catalyst toward reactions such as ethylene epoxidation.[8]

One viable approach to preserving the geometric shape of Ag nanocrystals is to passivate the most susceptible sites at edges with a relatively inert metal M for the generation of Ag@M core-frame nanocrystals. In general, the choice of M needs to fulfill the following requirements. First, M should be corrosion-resistant in an aqueous solution at all pH values. Second, M must have a much higher melting point than that of Ag (962 °C) to render the system greater thermal stability. Third, M should take a face-centered cubic (fcc) structure, together with a good match in lattice constant with Ag, to facilitate the conformal, epitaxial deposition of M on the Ag surface. Most of the platinum group metals (PGMs) are strong candidates for this application. It has been demonstrated that seeded growth offers a simple and versatile route to selectively deposit M on the edges of preformed Ag nanocrystals for the fabrication of Ag@M core-frame products.[9,10] In a typical process, a reducing agent is mixed with the Ag nanocrystals in a colloidal suspension, followed by dropwise titration of a precursor solution to metal M. By controlling the experimental conditions to eliminate self-nucleation, the M atoms derived from the chemical reduction can be selectively deposited on the edges of the seeds for the creation of bimetallic nanocrystals with a core-frame structure. In addition to the great improvement in shape stability, the inclusion of a small amount of PGM atoms also expand the catalytic capabilities of Ag nanocrystals. In particular, the core-frame nanocrystals can serve as a unique probe for the in situ detection and analysis of catalytic reactions through SERS fingerprinting.[11−13] Furthermore, upon selective removal of the Ag core by etching, the core-frame nanocrystals can be transformed into Ag-M nanoframes with a highly open structure for catalytic applications.[14,15] On the other hand, a core−shell nanocrystal can be obtained when the M atoms are conformally deposited over the entire surface.[16,17] After removal of the Ag core, the core−shell particles will be converted into nanoboxes and nanocages.[17,18] Although the M shell can also improve the shape stability of the nanocrystal, its surface and catalytic properties would be dominated by M rather than a combination of M and Ag. In addition, the products involving the core−shell configuration would require the use of more PGMs relative to the core-frame counterparts, significantly increasing the material cost. Altogether, it is believed that core-frame nanocrystals would be advantageous over core−shell and other variants in practical applications.

## 2. RATIONAL SYNTHESIS OF SILVER-BASED CORE-FRAME NANOCRYSTALS

Over the past decades, many groups have successfully synthesized Ag nanocrystals with a variety of shapes, including cubes, cuboctahedra, bipyramids, decahedra, icosahedra, plates or prisms, and rods or wires.[4,19−22] In general, the shape taken by nanocrystals in a solution-phase synthesis can be controlled through a thermodynamic or kinetic approach.[23] The thermodynamic control is typically attained through the use of a capping agent that can selectively bind to a facet to reduce its specific surface energy and thus promote a growth pathway that eventually leads to a maximum expression of this facet on the surface. For Ag nanocrystals with an fcc structure, the specific surface energies of low-index facets increase in the order $\gamma_{\{111\}} < \gamma_{\{100\}} < \gamma_{\{110\}}$ when there is no capping agent in the solution.[24] As a result, both the {110} and {100} facets should be gradually replaced by the {111} facets, leading to the formation of truncated cubes, cuboctahedra, and finally octahedra. However, if a capping agent toward the {100} facets is introduced into the reaction solution at an adequate concentration, nanocubes covered by the otherwise less stable {100} facets will be formed.[25] This concept has been demonstrated using the synthesis of Ag nanocubes in ethylene glycol (EG), with poly(vinylpyrrolidone) (PVP) serving as the surface capping agent.[19] Because PVP binds to the {100} facets most strongly, the specific surface energies of low-index facets increase in the order $\gamma_{\{100\}} < \gamma_{\{111\}} < \gamma_{\{110\}}$, leading to the formation of nanocubes enclosed by {100} facets.

Figure 1 illustrates two approaches to the transformation of a Ag nanocube into a Ag-based core-frame nanocube. The first strategy involves galvanic-free codeposition of M and Ag on the edges of a Ag nanocube. In a typical process, both $M^{n+}$ and $Ag^+$ precursors are cotitrated into an aqueous suspension of Ag nanocubes in the presence of ascorbic acid ($H_2Asc$, reducing agent) and PVP (colloidal stabilizer) at room temperature.[13,26] When the added $Ag^+$ ions can effectively retard the galvanic


https://doi.org/10.1021/accountsmr.1c00269
Acc. Mater. Res. 2022, 3, 391−402

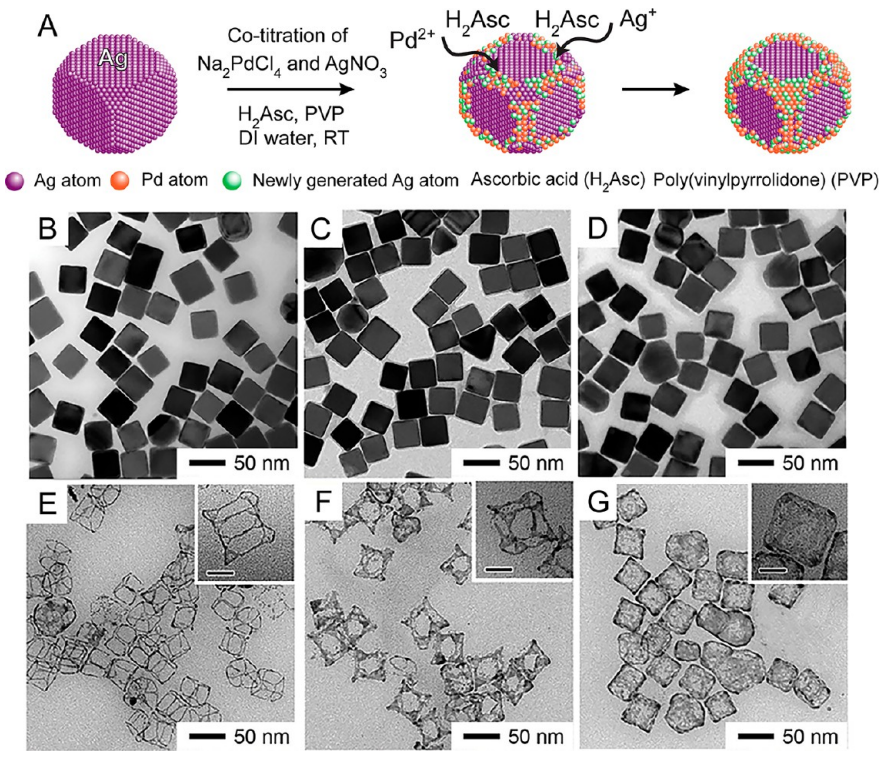


**Figure 2.** (A) Schematic illustration showing the transformation of a Ag nanocube into a Ag@Pd-Ag core-frame nanocube by cotitrating $Na_2PdCl_4$ and $AgNO_3$ into an aqueous suspension of Ag nanocubes in the presence of $H_2Asc$ and PVP. (B–D) TEM images of the as-prepared nanocubes when the cotitration volume of $AgNO_3$ (0.1 mM) and $Na_2PdCl_4$ (0.2 mM) is set to (B) 0.1 mL, (C) 0.2 mL, and (D) 0.3 mL, respectively, for each precursor solution. (E–G) TEM images of the resultant nanostructures after etching of the samples shown in (B–D) with aqueous $H_2O_2$. The scale bars in the insets are 20 nm. TEM images reproduced with permission from ref 13. Copyright 2015 American Chemical Society.

replacement reaction between $M^{n+}$ and Ag, the M and Ag atoms derived from the reduction of the two precursors by $H_2Asc$ will be codeposited on the edges of the Ag nanocube to generate a Ag@M-Ag core-frame nanocube. The second strategy involves a combination of carving of Ag from the side faces and then codeposition of M and Ag on the edges of a Ag nanocube in an site-orthogonal manner. In one protocol, the $M^{n+}$ precursor is titrated into an aqueous suspension of Ag nanocubes in the presence of $H_2Asc$, sodium hydroxide (NaOH, pH modifier), and cetyltrimethylammonium chloride (CTAC, colloidal stabilizer and surface capping agent) at room temperature.[27,28] Different from the first strategy that involves the use of PVP as a colloidal stabilizer only for the generation of Ag@Ag-M core-frame nanocubes, the $Cl^-$ ions from CTAC can selectively bind to the Ag(100) surface in an aqueous solution.[29] In this case, Ag atoms are carved from the side faces of Ag nanocubes through the galvanic replacement reaction between the Ag and the $M^{n+}$ precursor. Concurrently, M and Ag atoms are produced from the reduction of the $M^{n+}$ precursor and dissolved $Ag^+$ ions by the ascorbate monoanion ($HAsc^-$), a product of the neutralization reaction between $H_2Asc$ and NaOH, followed by their codeposition on the edges of a Ag nanocube, due to their higher surface energy, for the generation of a Ag@M-Ag concave nanocube.[28,30] In another protocol, the $M^{n+}$ precursor is titrated into a suspension of Ag nanocubes in ethylene glycol (EG) solution held at 110 °C in the presence of $H_2Asc$ and PVP.[31,32] As demonstrated in the synthesis of Ag nanocubes, PVP can selectively bind to the Ag(100) surface in an EG solution.[19,25] Similar to the aqueous synthesis of Ag@M-Ag concave cubes, where $Cl^-$ ions can selectively bind to the Ag(100) surface,[28] Ag atoms are carved from the side faces through the galvanic replacement reaction while the reduction of $M^{n+}$ and dissolved $Ag^+$ ions by both $H_2Asc$ and EG produces Ag and M atoms for their codeposition on the edges of a Ag nanocube, leading to the creation of a Ag@M-Ag core-frame concave nanocube.[32]

### 2.1. Galvanic-Free Codeposition for the Generation of Ag-Based Core-Frame Nanocrystals

Seeded growth has been extensively used for the synthesis of bimetallic nanocrystals bearing a core-frame structure.[9,10] This strategy is built upon the concept that preformed nanocrystals can serve as seeds for the heterogeneous nucleation and growth of a different metal. In the past, seeded growth has been successfully implemented when the seed is made of a less reactive metal than the one to be deposited.[9] However, when nanocrystals made of a relatively reactive metal such as Ag are employed as the seeds, Ag can spontaneously undertake galvanic replacement reaction with the precursors to Au, Pt, and Pd, destructing the capability of the seeds to faithfully direct the growth.[33] In a set of studies, my group addressed this issue by introducing a faster chemical reduction to compete with and thus suppress the galvanic replacement reaction.[13,16,26] Figure 2A illustrates one approach that involves the cotitration of $Na_2PdCl_4$ and $AgNO_3$ into an aqueous suspension of Ag nanocubes in the presence of $H_2Asc$ and PVP at room temperature.[13] When the molar ratio of $AgNO_3$ to $Na_2PdCl_4$ was greater than 0.5, the added $Ag^+$ ions could push the galvanic replacement reaction between Ag and $Na_2PdCl_4$ backward. As such, the reduction of the two precursors by $H_2Asc$ produced Pd and Ag atoms for their initial codeposition on the edges of a Ag nanocube, generating a Ag@Pd-Ag core-frame nanocube. As the reaction was continued, more and more Pd and Ag adatoms


https://doi.org/10.1021/accountsmr.1c00269
Acc. Mater. Res. 2022, 3, 391–402

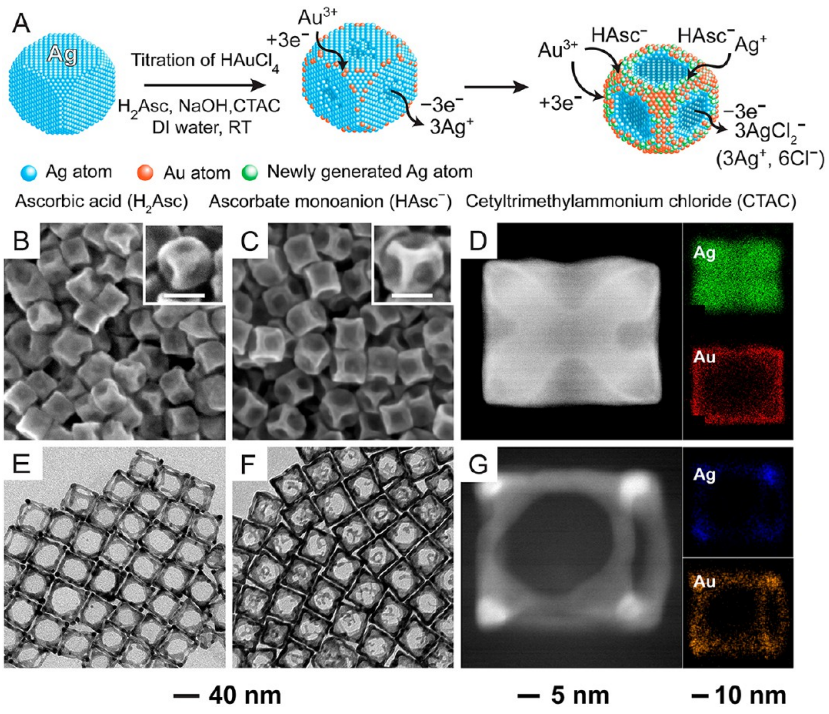


**Figure 3.** (A) Schematic illustration showing the transformation of a Ag nanocube into a Ag@Au-Ag core-frame concave nanocube by titrating $HAuCl_4$ into an aqueous suspension of Ag nanocubes in the presence of $H_2Asc$, NaOH, and CTAC. (B, C) TEM images of concave nanocubes prepared at different titration volumes of $HAuCl_4$ (0.1 mM): (B) 0.8 mL and (C) 1.6 mL. (D) HAADF-STEM image and EDS mapping of one concave cube shown in (C). (E, F) TEM images of the resultant nanoframes after etching the samples shown in (B) and (C) with aqueous $H_2O_2$. (G) HAADF-STEM image and EDS mapping of one nanoframe shown in (F). The scale bars in the insets are 40 nm. Reproduced with permission from ref 28. Copyright 2018 American Chemical Society.

would be generated for subsequent deposition on the corners and then side faces.

Panels B−D of Figure 2 show TEM images of the products obtained by cotitrating $AgNO_3$ (0.1 mM) and $Na_2PdCl_4$ (0.2 mM) up to volumes of 0.1, 0.2, and 0.3 mL, respectively, for each precursor solution. The absence of pits on the particles indicated that no galvanic replacement reaction between Ag and $Na_2PdCl_4$ was involved. When the as-prepared samples were etched with aqueous $H_2O_2$ to selectively remove Ag while leaving Pd intact, panels E−G of Figure 2 show different types of as-obtained nanostructures. At a titration volume of 0.1 mL, Figure 2E suggests that the resultant Pd atoms were only deposited on the edges, rather than the corners, of Ag nanocubes, for the formation of nanoframes with an ultrathin ridge thickness. When the titration volume was increased to 0.2 mL, Figure 2F shows the formation of nanoframes with thicker ridges, together with the presence of Pd atoms at the corners. When the titration volume was further increases to 0.3 mL, Figure 2G shows the formation of nanocages due to the coverage of Pd atoms on the edges, corners, and side faces. Altogether, these results confirm the progression of Pd deposition from edges to corners and then side faces of the Ag nanocubes as the titration volume was increased. It is worth mentioning that the frames were made of Ag and Pd alloys because Ag and Pd are completely miscible to each other. In addition, interatomic diffusion between Ag and Pd would also contribute to the formation of alloys. In another study, the capability of this cotitration method was extended to the synthesis of Ag@Au-Ag core-frame nanocubes, as well as their nanoframe derivatives.[26] Because the reduction potential of $AuCl_4^-$ is higher than that of $PdCl_4^{2-}$, the lower limit of the molar ratio between $AgNO_3$ and $HAuCl_4$ should be increased to 3 in order to effectively inhibit galvanic replacement reaction. More importantly, my group demonstrated that the added $HAuCl_4$ and $AgNO_3$ could be completely reduced to produce Ag and Au atoms, respectively, followed by their codeposition onto the edges of the Ag nanocubes. In general, it is feasible to control the composition of the Ag−Au alloy being deposited on the edges of Ag nanocubes by simply maneuvering the feeding ratio between the two precursors. It is arguable that this protocol can be further extended to the fabrication of Ag@M-Ag (M: Pt, Ir, Rh, and Ru) core-frame nanocrystals. These core-frame nanocubes embrace both plasmonic and catalytic properties for reporting on chemical reactions by SERS (see section 3.2).

### 2.2. Site-Selective Carving and Codeposition for the Generation of Ag-Based Core-Frame Concave Nanocrystals

In a different approach, site-selected carving and codeposition are integrated for the fabrication of Ag-based core-frame concave nanocubes.[28,32,34] The success of this method relies on the ability to confine oxidative etching of Ag from to the side faces while the codeposition of M and Ag only occurs on the edges of a nanocube in a site-orthogonal manner. In one example, Figure 3A illustrates the transformation of a Ag nanocube into a Ag@Au-Ag core-frame nanocube with a concaved surface.[28] In a typical process, $HAuCl_4$ (0.1 mM) was titrated into an aqueous suspension of Ag nanocubes in the presence of $H_2Asc$, NaOH, and CTAC at an initial pH of 11.6 and under ambient conditions. In this case, the oxidation of Ag was started from side faces due to their capping by $Cl^-$ ions. Concurrently, both $AuCl_4^-$ and the dissolved $Ag^+$ ions were reduced by $HAsc^-$ for the generation of Au and Ag atoms, followed by their initial codeposition on the edges and then corners of the Ag nanocube. Panels B and C of Figure 3 show SEM images of the Ag@Au-Ag concave nanocubes obtained


https://doi.org/10.1021/accountsmr.1c00269
Acc. Mater. Res. 2022, 3, 391−402

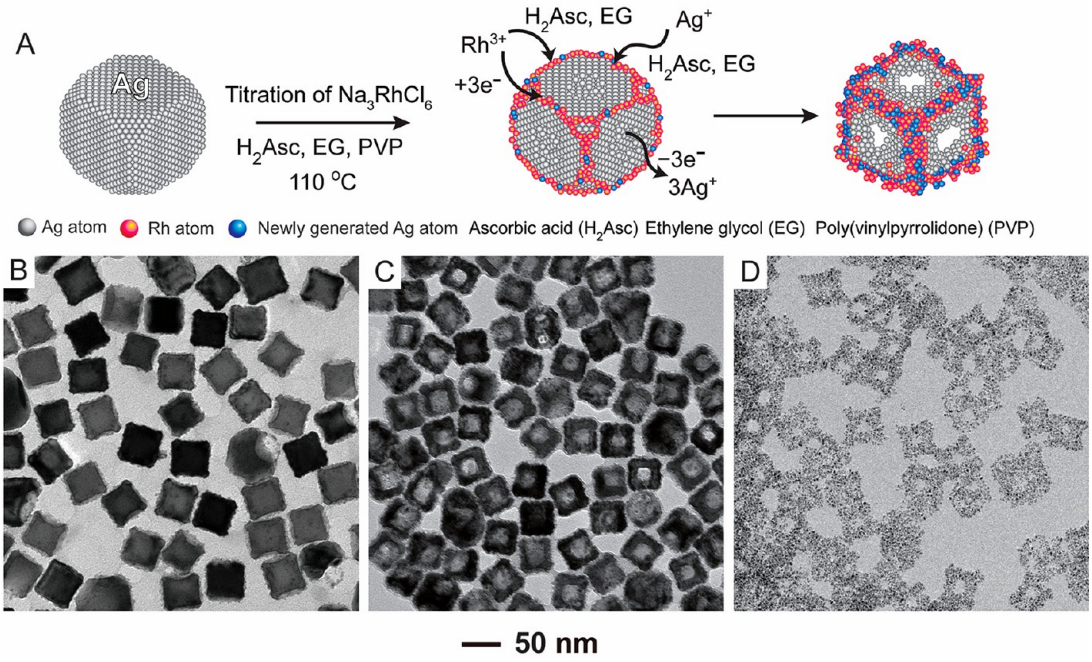


**Figure 4.** (A) Schematic illustration showing the transformation of a Ag nanocube into a Ag@Rh-Ag core-frame concave nanocube and a Ag−Rh hollow nanocube by titrating different volumes of the $Na_3RhCl_6$ solution into a suspension of Ag nanocubes in EG containing $H_2Asc$ and PVP. (B, C) TEM images of the nanostructures prepared by titrating (B) 0.1 mL and (C) 0.3 mL, respectively, of the $Na_3RhCl_6$ solution (2 mM). (D) TEM image of the resultant nanoframes after etching the sample shown in (C) with an aqueous solution of $Fe(NO_3)_3$ and $HNO_3$. Reproduced with permission from ref 32. Copyright 2019 American Chemical Society.

after the titration of 0.8 and 1.6 mL, respectively, of $HAuCl_4$. The nanocubes became more concave on their side faces as the titration volume of $HAuCl_4$ was increased. Figure 3D shows the aberration-corrected high-angle annular dark-field scanning TEM (HAADF-STEM) image recorded from one of the Ag@Au-Ag concave nanocubes shown in Figure 3C, together with the corresponding energy dispersive X-ray spectroscopy (EDS) elemental mapping. The regions with dark contrast in the HAADF-STEM image indicates the presence of concavity on the side faces due to the loss of Ag. The EDS results confirm the distribution of Ag and Au atoms in the core and at the edges and corners of the nanocube, respectively. To reveal the deposition of Au, these two samples were etched with aqueous $H_2O_2$. Panels E and F of Figure 3 show TEM images of the resultant nanostructures. Figure 3G shows the HAADF-STEM image of an individual Ag−Au nanoframe sampled from Figure 3F, together with the corresponding EDS elemental mapping of both Ag and Au. Altogether, these results confirm the deposition of Au on the edges and corners of the Ag nanocubes.

Per results from another study, Figure 4A shows the transformation of a Ag nanocube into a Ag@Rh-Ag core-frame concave nanocube and then a Ag−Rh hollow nanocube.[32] In a typical process, a solution of $Na_3RhCl_6$ in EG (2 mM) was titrated into a suspension of Ag nanocubes in EG held at 110 °C in the presence of $H_2Asc$ and PVP. Different from the aqueous system, the use of EG as a solvent helped address challenges associated with the instability of some metal precursors in an aqueous system because of hydrolysis.[35] It is also well-established that the reducing power of EG can be augmented by elevating the reaction temperature,[36] making the rate of chemical reduction faster than that of the galvanic replacement reaction. Like the reaction in the aqueous system with the involvement of CTAC as a surface capping agent, Ag atoms from the side faces were carved through oxidation while the reduction of $Na_3RhCl_6$ and the dissolved $Ag^+$ ions by both EG and $H_2Asc$ produced Rh and Ag atoms for their subsequent codeposition on the edges and corners of the nanocube in a site-orthogonal manner. Panels B and C of Figure 4 show TEM images of the as-obtained products when two different volumes of the $Na_3RhCl_6$ solution had been titrated. At 0.1 mL, Figure 4B shows the creation of nanocubes with concaved side faces and rough edges. At 0.3 mL, Figure 4C shows the formation of nanocubes with hollow interior and islands on the surface. After the sample shown in Figure 4C was etched with an aqueous mixture of $Fe(NO_3)_3$ and $HNO_3$, Figure 4D shows the formation of nanoframes, validating the preferential deposition of Rh atoms on the edges and corners of the Ag nanocubes.

In summary, cotitration of $Ag^+$ and $M^{n+}$ precursors offers a facile approach to the fabrication of Ag-based core-frame nanocrystals by retarding the galvanic replacement reaction between Ag and the $M^{n+}$ precursor while promoting the deposition of M and Ag on the edges and vertices of Ag nanocrystals. Alternatively, one can leverage the interplay between galvanic replacement and chemical reduction to achieve site-selective carving and codeposition for the generation of Ag-based core-frame concave nanocrystals.

## 3. UTILIZATION OF THE SILVER-BASED CORE-FRAME NANOCRYSTALS

This section discusses a few applications enabled or enhanced by the Ag-based core-frame nanocrystals. I will introduce the concept to preserve the geometric shape of Ag nanocubes at an elevated temperature by framing their edges with Ir. I will then highlight the use of Ag@Pd-Ag or Ag@Rh-Ag core-frame nanocubes as a bifunctional probe integrated with plasmonic and catalytic properties for catalyzing and reporting chemical reactions. Finally, I will discuss how to leverage the unique


https://doi.org/10.1021/accountsmr.1c00269
Acc. Mater. Res. 2022, 3, 391−402

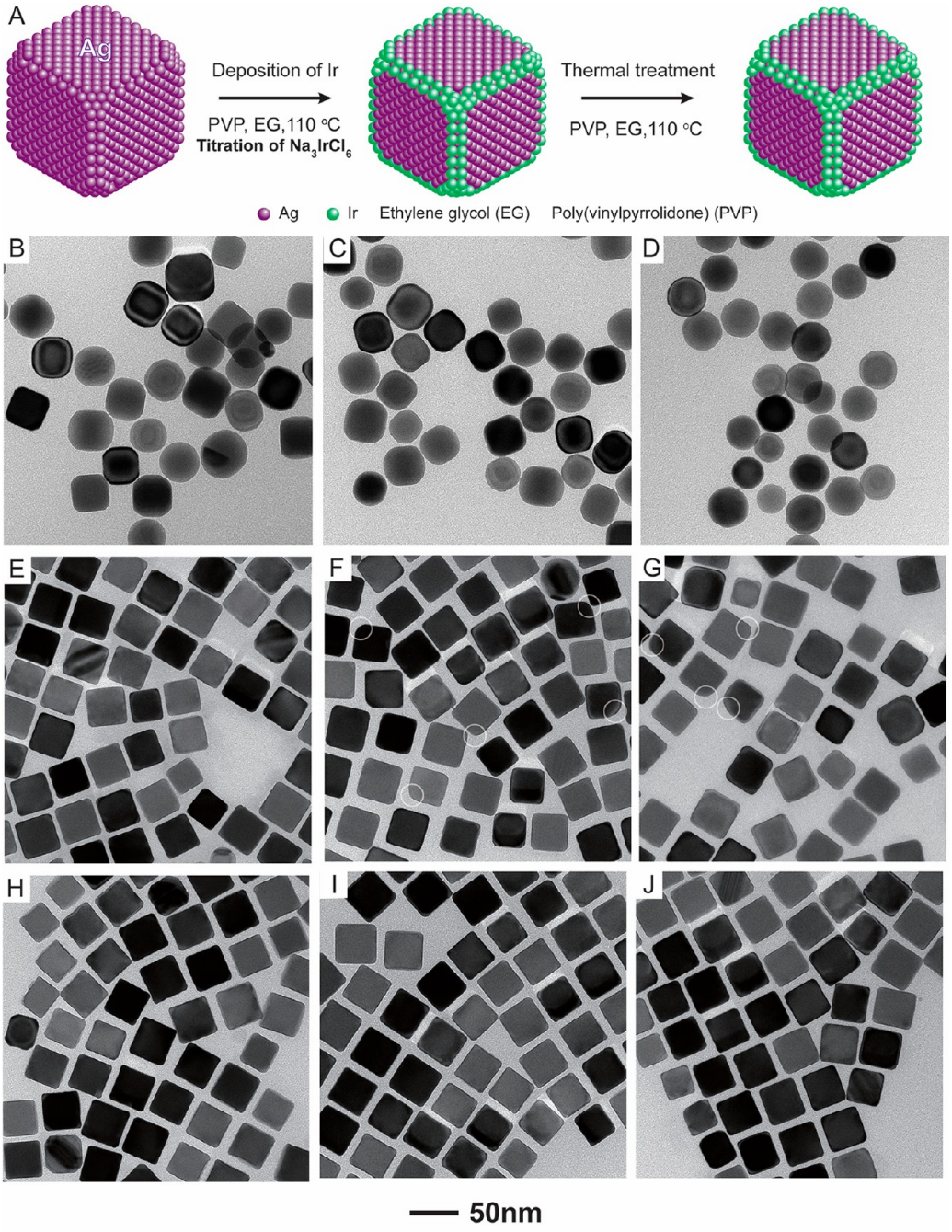


**Figure 5.** (A) Schematic illustration of the transformation of a Ag nanocube to a Ag−Ir core-frame nanocubes by titrating $Na_3IrCl_6$ in an EG solution (2 mM) into a suspension of Ag nanocubes in PVP/EG, followed by treatment in PVP/EG at 110 °C. (B−D) TEM images of Ag nanocubes that had been treated in a PVP/EG solution at 110 °C for (B) 5 min, (C) 10 min, and (D) 30 min, respectively. (E−G) TEM images of the Ag−Ir nanocubes prepared by titrating 0.05 mL of the $Na_3IrCl_6$ solution (E) before and after thermal treatment for (F) 10 min and (G) 30 min. (H−J) TEM images of the Ag−Ir nanocubes prepared by titrating 0.1 mL of the $Na_3IrCl_6$ solution (H) before and after thermal treatment for (I) 10 min and (J) 30 min. Reproduced with permission from ref 7. Copyright 2020 Royal Society of Chemistry.

composition of a Ag@Au-Ag core-frame nanocube to have it transformed into a nanoscale cage cube made of a trimetallic alloy through a galvanic replacement reaction.

### 3.1. Enhancing the Shape Stability of Ag Nanocrystals

As discussed previously, the Ag atoms located at the edges and corners of Ag nanocubes are most vulnerable to oxidation and dissolution, leading to their shape instability. In a recent study, my group demonstrated an effective strategy for preserving the shape of Ag nanocubes by covering their edges and corners with Ir.[7] As illustrated in Figure 5A, Ag nanocubes were dispersed in a PVP/EG solution, followed by titrating different volumes of the $Na_3IrCl_6$/EG solution (2 mM) at 110 °C. It was argued that $Na_3IrCl_6$ would be reduced for the generation of Ir atoms, followed by their deposition on the edges and then corners of the Ag nanocubes. The shape stabilities of the as-prepared Ag−Ir core-frame nanocubes were then evaluated by incubating the nanocubes in a PVP/EG solution at 110 °C. In the first set of experiments, the original Ag nanocubes were dispersed in a PVP/EG solution at 110 °C, followed by the collection of three


https://doi.org/10.1021/accountsmr.1c00269
Acc. Mater. Res. 2022, 3, 391−402

samples at 5, 10, 30 min, respectively, for TEM characterization. Panels B–D of Figure 5 show TEM images of the resultant particles at three time points, suggesting the transformation of nanocubes to nanospheres. In the second set of experiments, 0.05 mL of $Na_3IrCl_6$ was titrated into the reaction solution. Figure 5E shows a TEM image of the product. The sharpened corners on the nanocubes indicated the deposition of Ir. Panels F and G of Figure 5 show TEM images of the resultant nanoparticles after incubating the sample shown in Figure 5E in PVP/EG at 110 °C for 10 and 30 min, respectively. Truncations could be identified at a limited number of corners as marked by circles, likely due to the insufficient coverage of Ir. In the third set of experiments, the titration volume of $Na_3IrCl_6$ was increased to 0.1 mL. Figure 5H shows TEM image of the product with a cubic shape. Panels H and J of Figure 5 show the resultant nanoparticles after the sample shown in Figure 5H had been incubated in PVP/EG at 110 °C for 10 and 30 min, respectively. In these cases, the cubic shape of these nanocubes was well preserved. Evidently, the increased number of Ir atoms deposited on the edges and corners of the nanocubes greatly improved the shape stability. Inductively coupled plasma mass spectrometry (ICP-MS) was further used to measure the Ir contents in these two samples. It was found that the Ir to Ag atomic ratios of these two samples were 1:241 and 1:165, respectively. Collectively, these results conclude that the deposition of Ir on the edges and corners of Ag nanocubes can prevent the Ag atoms from oxidation and thereby preserve their cubic shape at an elevated temperature. It is anticipated that the deposition of a PGM can also introduce new catalytic properties while enhancing the thermal stability of the Ag nanocrystals.

### 3.2. Bifunctional Core-Frame Nanocrystals with Integrated Plasmonic and Catalytic Properties

Although Ag nanocrystals embrace superior LSPR properties in the visible region for SERS applications, they can only catalyze specific oxidation reactions such as ethylene epoxidation.[37] In comparison, PGMs such as Pd, Rh, Pt, Ir, and Ru are good catalysts toward a variety of chemical reductions,[38] but their plasmonic properties are compromised because of the weak coupling between their conduction electrons and visible light.[39] In a set of studies, my group demonstrated the concept to decorate the edges of Ag nanocrystals with PGMs for the creation of Ag-based core-frame nanocubes with integrated SERS and catalytic properties on the same nanocrystal.[13,32] Figure 6A illustrates the use of Ag@Pd-Ag core-frame nanocubes for catalyzing and probing chemical reactions.[11,13,40] These bimetallic nanocubes were synthesized by following the protocols described in section 2.1. In the first step, 4-nitrothiophenol (4-NTP) molecules adsorb on the Ag surface in the proximity to the SERS hot spots located on the edges of the core-frame nanocube through the Ag–S linkage. When the 4-NTP-modified nanocubes were mixed with $NaBH_4$ in an aqueous solution under ambient conditions, $NaBH_4$ would decompose to produce $H_2$, followed by their adsorption and dissociation on the Pd surface to generate H atoms.[41] The atomic hydrogen could quickly reduce 4-NTP to 4-aminethiophenol (4-ATP). The 4-ATP molecules could remain on the surface of the core-frame nanocubes until all the $NaBH_4$ in the reaction solution had completely decomposed. Afterward, the Ag surface activated the $O_2$ from air,[42] enabling Ag-catalyzed oxidation of 4-ATP to *trans*-4,4′-dimercaptoazobezene (*trans*-DMAB).

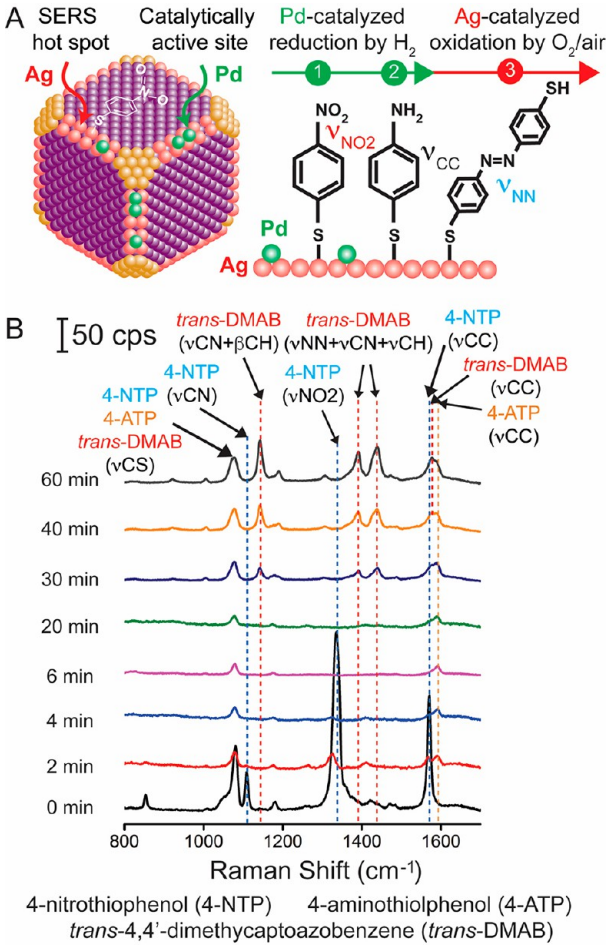


**Figure 6.** (A) Schematic illustration of the Pd adatoms on the edges of a Ag nanocube for catalyzing and reporting on the sequential Pd-catalyzed reduction of 4-NTP to 4-ATP by hydrogen and the Ag-catalyzed oxidation of 4-ATP to *trans*-DMAB by $O_2$ in the air using SERS. (B) Time-dependent SERS spectra recorded from an aqueous suspension of 4-NTP-functionalized Ag@Pd-Ag core-frame nanocubes with 4.6 wt % Pd before and after the introduction of the $NaBH_4$ solution. (A) Reproduced with permission from ref 11. Copyright 2020 Wiley-VCH Verlag GmbH & Co. (B) Reproduced with permission from ref 40. Copyright 2016 Wiley-VCH Verlag GmbH & Co.

Figure 6B shows the time-dependent SERS spectra recorded from an aqueous suspension of the Ag@Pd-Ag nanocubes containing 4.6 wt % Pd at different time points.[40] Initially, the three vibrational peaks at 1108, 1336, and 1572 $cm^{-1}$ (marked by dashed blue lines) were assigned to the $\nu_{CN}$, $\nu_{NO_2}$, and $\nu_{CC}$ bands of 4-NTP, respectively. At $t$ = 2 min after the addition of $NaBH_4$, the $\nu_{NO_2}$ band was slightly red-shifted while the $\nu_{CC}$ band of 4-ATP appeared at 1595 $cm^{-1}$ (marked by a dashed orange line), confirming the reduction of 4-NTP to 4-ATP. On the other hand, other bands of 4-NTP remained at essentially the same peak positions while showing significant reduction in peak intensity. It was argued that the added $NaBH_4$ could promote the desorption of 4-NTP from the surface.[43] When the reaction progressed to $t$ = 4 min, all the bands associated with 4-NTP disappeared, indicating the completion transformation of 4-NTP to 4-ATP. From $t$ = 4–20 min, the SERS spectra showed little change. At $t$ = 30 min, three bands appeared at 1142, 1388, and 1429 $cm^{-1}$ (marked by dashed red lines), with their assignment to the $\nu_{CN} + \beta_{CH}$, $\nu_{NN} + \nu_{CN}$, and $\nu_{NN} + \beta_{CH}$ of *trans*-


https://doi.org/10.1021/accountsmr.1c00269
Acc. Mater. Res. 2022, 3, 391–402

DMAB, respectively. This result suggests that the conversion of 4-ATP to *trans*-DMAB by the $O_2$ from the air once the $NaBH_4$ in the solution had been depleted. The spectrum remained essentially unchanged up to $t$ = 60 min. Collectively, this study demonstrated that the Ag@Pd-Ag core-frame nanocubes could serve as a dual catalyst while reporting on the conversion of an aromatic nitro compound to an aromatic azo compound by SERS.

In another study, Ag@Rh-Ag core-frame nanocubes with 2.84 wt % Rh content were utilized to catalyze the degradation of environmental pollutants while monitoring the reaction by SERS.[32] Specifically, the protocol described in section 2.2 was used to synthesize the core-frame nanocubes. After their surface was functionalized with Rhodamine 6G (R6G), SERS spectra were collected at different time points after the introduction of $NaBH_4$. Figure 7A shows the time-dependent SERS spectra after the removal of fluorescence background. At the beginning, the characteristic peaks of R6G were resolved at 612 $cm^{-1}$ (in-plane xanthene ring deformations), 775 $cm^{-1}$ (in plane xanthene ring deformations), 1364 $cm^{-1}$ (xanthene ring stretch), 1510 $cm^{-1}$ (xanthene ring stretch), and 1642 $cm^{-1}$ (xanthene ring stretch), respectively. At $t$ = 2 min post the addition of $NaBH_4$, the peak intensities of all these bands decreased. At $t$ = 6 min, the peak intensities dropped by almost 70%. By $t$ = 8 min, none of these peaks could be detected, suggesting the complete degradation of R6G. In comparison, when the Ag@Rh-Ag nanocubes were replaced with Ag nanocubes while keeping all other experimental parameters unchanged, Figure 7B shows that a series of SERS spectra recorded over a period up to 30 min, indicating that these spectra remained essentially the same. Altogether, these results confirm that the Rh atoms situated on the surface of the Ag@Rh-Ag nanocubes were able to catalyze the degradation of R6G by $NaBH_4$.

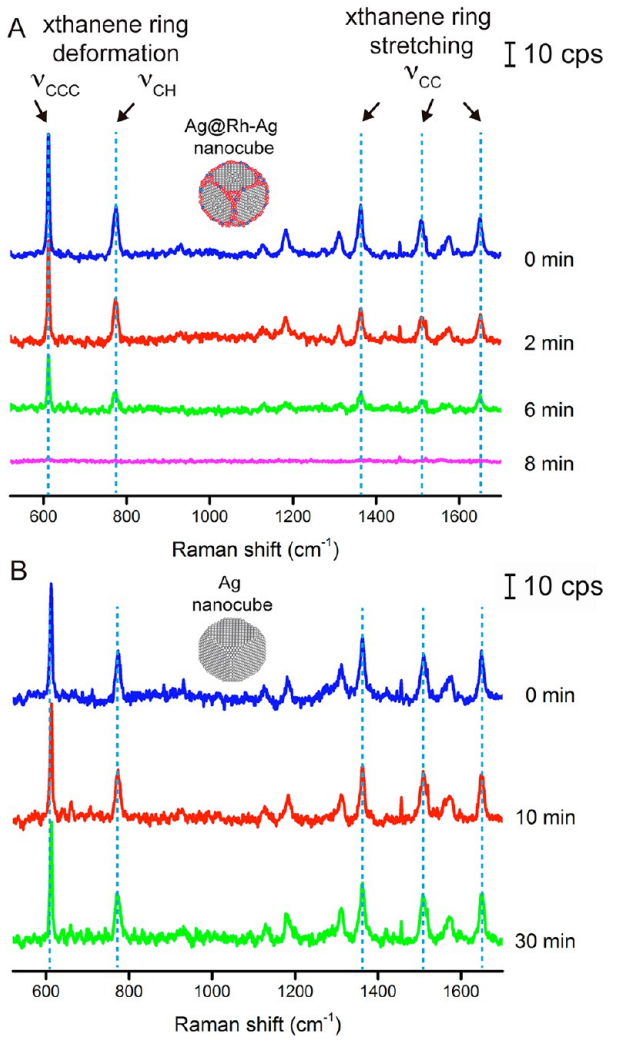


**Figure 7.** (A, B) Time-dependent SERS spectra recorded before and after the introduction of the $NaBH_4$ solution into an aqueous suspension containing (A) R6G-functionalized Ag@Rh-Ag nanocubes with 2.84 wt % Rh content and (B) R6G-functionalized Ag nanocubes. Reproduced with permission from ref 32. Copyright 2019 American Chemical Society.

In summary, when the edges of Ag nanocubes are decorated with a PGM element, the resultant core-frame nanocubes with integrated plasmonic and catalytic activities can catalyze a reaction while reporting on the chemical species involved through SERS fingerprinting. Most recently, my group reported another strategy to expand the catalytic capacity of Ag nanocrystals by modifying their surface with an organic ligand. It was demonstrated that isocyanide compounds could adsorb on the surface of Ag nanocubes to promote Ag-catalyzed redox reactions between isocyanide and nitroaromatic molecules toward the production of an aromatic azo compound.[44]

### 3.3. Selective Etching of Ag from Ag-Based Core-Frame Nanocrystals by Controlling Their Landscape of Composition

As discussed in section 2, a Ag nanocube can be transformed into a bimetallic core-frame concave nanocube with well-defined, spatially controlled distributions of elements on its surface. In a recent study, my group demonstrated the feasibility of galvanic replacement reaction between a bimetallic core-frame concave nanocube and a third metal precursor for the generation of a multimetallic cage cube.[45] Figure 8A illustrates the transformation of a Ag@Au-Ag core-frame concave nanocube into a Ag−Au−Pt concave nanocube and then a Ag−Au−Pt cage cube. In a typical process, the as-prepared Ag@Au-Ag core-frame concave nanocubes were dispersed in an aqueous solution of CTAC, followed by the titration of an aqueous $H_2PtCl_6$ at room temperature. Because of the galvanic reaction between Ag and $H_2PtCl_6$ to produce one Pt atom at the expenses of four Ag atoms, Ag atoms were removed from the Ag-dominated regions located at the center of each side face of a nanocube while the Pt atoms were deposited on the edges and corners of the nanocube in a site-orthogonal manner. Once a thin layer of Ag−Au−Pt alloy was formed around the cavities but not inside the cavities, continuous carving of Ag along the center of a core-frame nanocube created a cage cube made of a Ag−Au−Pt alloy and characterized by three orthogonal, intersected holes.

After 1.2 mL of $H_2PtCl_6$ had been titrated into the suspension of Ag@Au-Ag core-frame concave nanocubes prepared with 0.8 mL of $HAuCl_4$ using the protocol described in section 2.2 (see Figure 3B), Figure 8B shows an SEM image of the Ag−Au−Pt cage cubes. Figure 8C gives the HAADF-STEM image of one cage cube oriented along the ⟨001⟩ zone axis. The same cage cube was then subjected to EDS mapping. Panels D−G Figure 8 provide the spatial distribution of Ag, Au, Pt, and Cl, respectively. It was found that the Ag followed the profile of the nanoparticle while both Au and Pt were predominantly distributed on the edges and corners of the cage cube. The weaker signal of Pt relative to those of Ag and Au indicated the


https://doi.org/10.1021/accountsmr.1c00269
Acc. Mater. Res. 2022, 3, 391−402

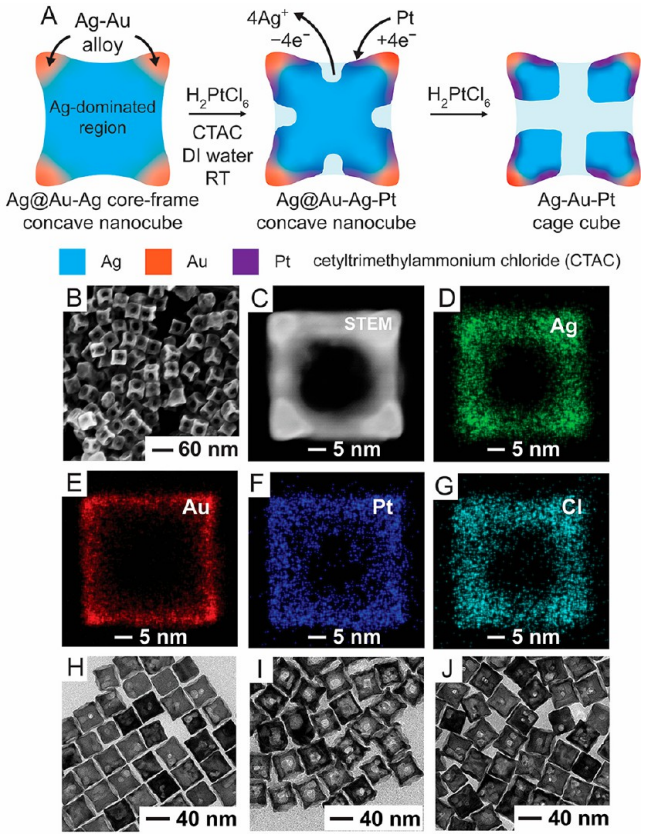


**Figure 8.** (A) Schematic diagram showing the transformation of a Ag@Au-Ag core-frame concave nanocube to a Ag@Au-Ag-Pt concave cube and then a Ag−Au−Pt cage cube by titrating $H_2PtCl_6$ (0.2 mM) into an aqueous suspension of Ag@Au-Ag core-frame concave nanocubes in the presence of CTAC. (B) SEM image of the Ag−Au−Pt cage cubes. (C) HAADF-STEM image of one Ag−Au−Pt cage cube shown in (B). The scale bar in the inset of (B) is 40 nm. (D−G) EDS elemental mapping of (D) Ag, (E) Au, (F) Pt, and (G) Cl of the Ag−Au−Pt cage cube in (C). (H−J) TEM images of the products that were obtained by reacting the Ag@Au-Ag concave nanocubes with (H) 0.4 mL of $K_2PtCl_4$ (0.2 mM), (I) 0.4 mL of $Na_2PdCl_4$ (0.2 mM), and (J) 0.24 mL of $HAuCl_4$ (0.2 mM), respectively. Reproduced with permission from ref 45. Copyright 2019 American Chemical Society.

limited deposition of Pt atoms. The overlap between the signal of Cl with that of Ag suggested that the $Cl^-$ ions derived from CTAC could bind to the Ag surface.[29,46] My group further demonstrated that the same strategy could be extended to other salt precursors for the creation of trimetallic cage cubes.[45] Panels H−I of Figure 8 show the three products obtained by replacing $H_2PtCl_6$ with $K_2PtCl_4$, $Na_2PdCl_4$, and $HAuCl_4$ while keeping other parameters the same as those in the standard protocol, respectively. Figure 8H shows the formation of cage cubes with relatively small holes in the center. In this case, one Pt atom was created at the expense of two Ag atoms, making carving of Ag less effective. When $K_2PtCl_4$ was replaced with $Na_2PdCl_4$, Figure 8I shows a TEM image of the product, indicating the creation of cage cubes with holes larger than those obtained from $K_2PtCl_4$. Likely, the difference in reduction potential of these two precursors would contribute to such a change in hole size. When $HAuCl_4$ was used to produce one atom at the expense of three Ag atoms through a galvanic replacement reaction, Figure 8J shows a TEM image of the product that includes Ag nanocubes with pits on their surfaces. Taken together, these results suggest that the size of the holes in the cage cubes can be tailored depending on the stoichiometry involved in the galvanic replacement reaction.

## 4. CONCLUSIONS AND OUTLOOK

Shape-controlled synthesis offers a powerful route to tailor the physicochemical properties of Ag nanocrystals, ultimately optimizing their performance in a broad spectrum of applications. Despite remarkable success, the full potential of shape-controlled Ag nanocrystals is yet to be fully realized because the sharp edges and corners on their surface are highly susceptible to truncation due to oxidative etching. The change in shape will cause significant deterioration to the electronic, optical, and catalytic properties of the nanocrystals. One approach to addressing this issue is to protect the vulnerable sites with a corrosion-resistant metal to generate Ag-based core-frame nanocrystals. This Account discussed two strategies for the rational synthesis of Ag-based nanocubes with a core-frame structure. The first strategy relied on the cotitration of a precursor to metal M and $AgNO_3$ into an aqueous suspension of Ag nanocubes in the presence of $H_2Asc$ and PVP, promoting galvanic-free codeposition of Ag and M atoms along the edges of Ag nanocubes for the generation of Ag@M-Ag core-frame nanocubes. In the second strategy, a precursor to M was titrated into a suspension of Ag nanocubes in the presence of $H_2Asc$ and CTAC in an aqueous solution under ambient conditions or in a EG/PVP system at an elevated temperature, respectively, carving Ag atoms from the side faces while codepositing of M and Ag atoms on the edges of the Ag nanocubes in a site-orthogonal manner for the creation of Ag@M-Ag core-frame concave nanocubes. The enhanced properties and applications of the Ag-based core-frame nanocubes were then highlighted using three case studies. In the first case, the edges and corners of Ag nanocubes were framed with a small number of Ir atoms to greatly enhance their shape stability at an elevated temperature. In the second case, Ag@Pd-Ag core-frame nanocubes were explored as a dual catalyst for monitoring the stepwise Pd-catalyzed chemical reduction and Ag-catalyzed oxidation by SERS. In the third case, Ag@Au-Ag core-frame concave nanocubes with well-controlled distribution of Au on the surfaces were transformed into Ag−Au−Pt trimetallic cage cubes through site-selective etching of Ag via a galvanic replacement reaction.

Moving forward, one can leverage the success in the development of Ag-based core-frame nanocubes to Ag nanocrystals with other shapes. In particular, one can deposit the second metal M on Ag pentagonal nanorods with tunable LSPR peaks in the NIR region.[47] The side surface of a pentagonal nanorod is enclosed by five {100} facets while the two ends are terminated in ten {111} facets. Since the twin boundaries between these facets are relatively higher in surface free energy than both {100} and {111} facets, they would be most favorable for the deposition of M for the creation of a Ag-based core-frame nanorod. In practice, one can achieve the desired growth by further optimizing the reaction temperature and the titration rate of the precursor to M used in the original protocols developed for the deposition of M on Ag nanocubes. It is anticipated that the core-frame nanorods should display LSPR peaks similar to those of Ag nanorods while integrating the catalytic properties of metal M, greatly expanding the spectral range for SERS-based detection of chemical reactions from the visible to the NIR region.

It is also worth mentioning that, despite the success in the fabrication of bimetallic systems in a core-frame structure, it is


https://doi.org/10.1021/accountsmr.1c00269
Acc. Mater. Res. 2022, 3, 391−402

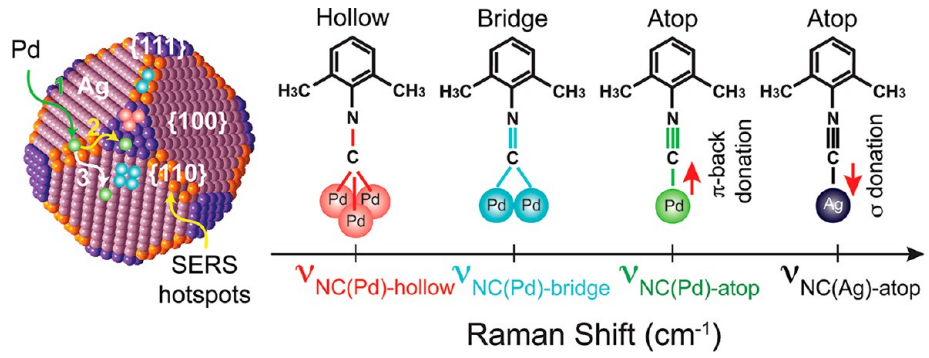


**Figure 9.** Illustration of SERS fingerprinting for monitoring the deposition of Pd atoms on a Ag nanocube. Reproduced with permission from ref 51. Copyright 2018 American Chemical Society.

difficult to detect and quantify the second metal being deposited on the surface of nanocrystal-based seeds while they are still suspended in the reaction medium. Today, it remains a daunting challenge to resolve the surface atomic composition during a solution-phase synthesis by all the imaging- or diffraction-based techniques.[48,49] In a set of recent studies, my group started to address this challenge by forging a paradigm shift through the development of isocyanide-based probes for investigating the heterogeneous nucleation and growth of the second metal such as Pt and Pd on Ag nanocrystals. In the proof-of-concept demonstration, my group established the use of 2,6-dimethylphenyl isocyanide (2,6-DMPI) as a molecular probe to monitor the deposition of Pt on the edges of Ag nanocubes in the original reaction solution by SERS.[50] Because the hot spots for SERS and the sites for initial deposition coincide at the edges of a Ag nanocube, in situ SERS embraces the sensitivity to detect as few as 27 Pt atoms being deposited onto the edge of a 39 nm Ag nanocube. In another study, it was established that 2,6-DMPI could bind to Pd atoms in three distinct configurations to provide a more detailed picture about atomic arrangement of Pd adatoms.[51] Figure 9 illustrates the concept, with 2,6-DMPI serving as a spectroscopic probe to elucidate the states of Pd atoms on the edges of a Ag nanocube, as well as the diffusion of Pd adatoms to corners and side faces. The isocyanide group of 2,6-DMPI binds to Ag and Pd via $\sigma$ donation and $\pi$-back-donation, respectively, leading to distinct positions for the $\nu_{NC(Ag)}$ and $\nu_{NC(Pd)}$ bands. In addition, isocyanide can bind to one, two, and three adjacent Pd atoms for the generation of atop, bridge, and hollow configurations, respectively, giving rise to $\nu_{NC(Pd)\text{-atop}}$, $\nu_{NC(Pd)\text{-bridge}}$, and $\nu_{NC(Pd)\text{-hollow}}$ bands with a continuing shift toward lower frequencies. By monitoring the evolution of $\nu_{NC}$ bands as a function of time, it was feasible to watch and track the early stage deposition of Pd on Ag nanocubes in real time. Most importantly, this in situ technique opens the door to investigating the explicit roles played by the reaction temperature and type of Pd precursor in affecting the growth of Pd−Ag bimetallic nanocrystals.

The power of the isocyanide probe can be further expanded to investigate the coreduction of precursors to two (or even more) different metals for their codeposition on Ag nanocubes by analyzing the outermost surface consisting of the deposited atoms and remaining Ag atoms by SERS. In principle, the isocyanide probe could characterize the composition of the outmost surface layer of Ag-based bimetallic nanocrystals by SERS at a sensitivity greater than that of electron microscopy. For example, 1,4-phenylene diisocyanide (1,4-PDI) was utilized to characterize the transformation of Ag@Au core−shell nanocubes from a Ag-dominated to a Au-enriched outermost surface when the Au shell thickness was increased from four to six atomic layers.[31] In the case of coreduction, depending on the difference in reaction kinetics between the precursors, two possible deposition patterns can be involved. If the precursors have different reduction kinetics, the precursor with a faster reduction rate should be deposited first, followed by the slower one. In contrast, when the precursors have comparable reduction kinetics, they are reduced concurrently for the codeposition of their atoms as an alloy. In principle, one can introduce 2,6-DMPI into the reaction solution to resolve the deposition pattern. For example, in a case study involving Pd and Rh, it will be feasible to resolve the distinct vibrational peaks at 2110 $cm^{-1}$ (atop) and 2130 $cm^{-1}$ for the NC group binding to Pd and Rh atoms, respectively.[51,32] In a typical experiment, $PdCl_4^{2-}$ and $RhCl_6^{3-}$ can be mixed at a 1:1 molar ratio and then titrated into an aqueous suspension of Ag nanocubes. More specifically, an aqueous mixture of the precursors will be titrated at an incremental volume. After the precursor mixture has been added, aliquots will be sampled from the reaction solution at different time intervals for SERS measurements. From the intensities of SERS peaks located at 2110 and 2130 $cm^{-1}$, one can derive the relative numbers of Pd and Rh atoms deposited on the edges of Ag nanocubes as a functional of the reaction time. The same measurement can be repeated by increasing the titration volume of the precursor mixture to different values. An analysis of the SERS spectra will reveal the codeposition pattern as a function of the volume of precursor mixture added into the growth solution. One can further vary the molar ratio of $PdCl_4^{2-}$ to $RhCl_6^{3-}$ from 1:1 to 10:1, 5:1, 1:5, and 1:10 to examine how this parameter will affect the codeposition pattern. Taken together, this set of experiments will point toward the codeposition pattern when a specific amount of a mixture of $PdCl_4^{2-}$ and $RhCl_6^{3-}$ at a certain molar ratio is titrated into an aqueous suspension of Ag nanocubes. The same study can also be extended to other combinations of metals, including Pd, Pt, Rh, Ir, and Ru. Such a quantitative understanding will provide invaluable insight and guidance for the rational synthesis of bi- and multimetallic nanocrystals with desired and controlled properties.

## AUTHOR INFORMATION

### Corresponding Author

**Dong Qin** − *School of Materials Science and Engineering, Georgia Institute of Technology, Atlanta, Georgia 30332, United States;* orcid.org/0000-0001-5206-5912; Email: dong.qin@mse.gatech.edu



https://doi.org/10.1021/accountsmr.1c00269
*Acc. Mater. Res.* 2022, 3, 391−402

Complete contact information is available at:
https://pubs.acs.org/10.1021/accountsmr.1c00269

## Funding

This work was supported by the National Science Foundation (CHE-1412006, CHE-1708300, and CHE-2002653), the ACS Petroleum Research Fund (PRF# 59664-ND10), and startup funds from the Georgia Institute of Technology.

## Notes

The author declares no competing financial interest.

## Biography

**Dong Qin** is an Associate Professor of Materials Science and Engineering at Georgia Tech, with an adjunct appointment in the School of Chemistry and Biochemistry. Her academic records include a B.S. in Chemistry from Fudan University (1990), a Ph.D. in Physical Chemistry with Professor Hai-Lung Dai from University of Pennsylvania (1996), a postdoctoral stint with Professor George M. Whitesides at Harvard University (1996−1997), and an MBA from the University of Washington (2003). Before joining Georgia Tech in 2012, she held administrative positions as Associate Dean for Research in the School of Engineering and Applied Science at Washington University in St. Louis (2007−2011) and Associate Director of Center for Nanotechnology at the University of Washington (2002−2007). She is an Associate Editor of Nanoscale and Nanoscale Advance, Royal Society of Chemistry (RSC), and she was elected a Fellow of Royal Society of Chemistry (FRSC) in 2021. Her research group pioneered a set of in situ techniques for the characterization of atomic/molecular events on the surface of noble-metal nanocrystals in a liquid phase and under operando conditions. Her group is also widely recognized for many original contributions to the rational synthesis of metal nanocrystals with unique properties.

## ■ ACKNOWLEDGMENTS

D.Q. thanks all the current and former group members for their contributions to this work.

## ■ REFERENCES

(1) Rycenga, M.; Cobley, C. M.; Zeng, J.; Li, W.; Moran, C. H.; Zhang, Q.; Qin, D.; Xia, Y. Controlling the Synthesis and Assembly of Silver Nanostructures for Plasmonic Applications. *Chem. Rev.* **2011**, *111*, 3669−3712.
(2) Willets, K. A.; Van Duyne, R. P. Localized Surface Plasmon Resonance Spectroscopy and Sensing. *Annu. Rev. Phys. Chem.* **2007**, *58*, 267−297.
(3) Christopher, P.; Xin, H.; Linic, S. Visible-Light-Enhanced Catalytic Oxidation Reactions on Plasmonic Silver Nanostructures. *Nat. Chem.* **2011**, *3*, 467−472.
(4) Wiley, B.; Sun, Y.; Xia, Y. Synthesis of Silver Nanostructures withControlled Shapes and Properties. *Acc. Chem. Res.* **2007**, *40*, 1067−1076.
(5) Rycenga, M.; Xia, X.; Moran, C. H.; Zhou, F.; Qin, D.; Li, Z.-Y.; Xia, Y. Generation of Hot Spots with Silver Nanocubes for Single-Molecule Detection by Surface-Enhanced Raman Scattering. *Angew. Chem., Int. Ed.* **2011**, *50*, 5473−5477.
(6) McLellan, J. M.; Siekkinen, A.; Chen, J.; Xia, Y. Comparison of the Surface-Enhanced Raman Scattering on Sharp and Truncated Silver Nanocubes. *Chem. Phys. Lett.* **2006**, *427*, 122−126.
(7) Wang, P.; Gao, R.; Qin, D. Preserving the Shape of Silver Nanocubes under Corrosive Environment by Covering their Edges and Corners with Iridium. *Nanoscale* **2020**, *12*, 20859−20867.
(8) Christopher, P.; Linic, S. Shape- and Size-Specific Chemistry of Ag Nanostructures in Catalytic Ethylene Epoxidation. *ChemCatChem.* **2010**, *2*, 78−83.
(9) Gilroy, K. D.; Ruditskiy, A.; Peng, H.-C.; Qin, D.; Xia, Y. Bimetallic Nanocrystals: Syntheses, Properties, and Applications. *Chem. Rev.* **2016**, *116*, 10414−10472.
(10) Wu, Y.; Sun, X.; Yang, Y.; Li, J.; Zhang, Y.; Qin, D. Enriching Silver Nanocrystals with a Second Noble Metal. *Acc. Chem. Res.* **2017**, *50*, 1774−1784.
(11) Shi, S.; Qin, D. Bifunctional Metal Nanocrystals for Catalyzing and Reporting on Chemical Reactions. *Angew. Chem., Int. Ed.* **2020**, *59*, 3782−3792.
(12) Zhang, Y.; Wu, Y.; Qin, D. Rational Design and Synthesis of Bifunctional Metal Nanocrystals for Probing Catalytic Reactions by Surface-Enhanced Raman Scattering. *J. Mater. Chem. C* **2018**, *6*, 5353−5362.
(13) Li, J.; Liu, J.; Yang, Y.; Qin, D. Bifunctional Ag@Pd-AgNanocubes for Highly Sensitive Monitoring of Catalytic Reactions by Surface-Enhanced Raman Spectroscopy. *J. Am. Chem. Soc.* **2015**, *137*, 7039−7042.
(14) Yang, T.-H.; Ahn, J.; Shi, S.; Gao, R.; Qin, D. Noble-Metal Nanoframes and Their Catalytic Applications. *Chem. Rev.* **2021**, *121*, 796−833.
(15) Li, J.; Sun, X.; Qin, D. Ag-Enriched Ag-Pd Bimetallic Nanoframes and Their Catalytic Properties. *ChemNanoMat* **2016**, *2*, 494−499.
(16) Yang, Y.; Liu, J.; Fu, Z.; Qin, D. Galvanic Replacement-Free Deposition of Au on Ag for Core-Shell Nanocubes with Enhanced Chemical Stability and SERS Activity. *J. Am. Chem. Soc.* **2014**, *136*, 8153−8156.
(17) Sun, X.; Yang, X.; Zhang, Y.; Ding, Y.; Su, D.; Qin, D. Pt−Ag Cubic Nanocages with Wall Thickness Less Than 2 nm and Their Enhanced Catalytic Activity Toward Oxygen Reduction. *Nanoscale* **2017**, *9*, 15107−15114.
(18) Sun, X.; Kim, J.; Gilroy, K. D.; Liu, J.; König, T. A. F.; Qin, D. Gold-Based Cubic Nanoboxes with Well-Defined Openings at the Corners and Ultrathin Walls Less Than Two Nanometers Thick. *ACS Nano* **2016**, *10*, 8019−8025.
(19) Sun, Y.; Qin, D. Shape-Controlled Synthesis of Gold and Silver Nanoparticles. *Science* **2002**, *298*, 2176−2179.
(20) Tao, A.; Sinsermsuksakul, P.; Yang, P. Polyhedral Silver Nanocrystals with Distinct Scattering Signatures. *Angew. Chem., Int. Ed.* **2006**, *45*, 4597−4601.
(21) Pietrobon, B.; Kitaev, V. Photochemical Synthesis of Monodisperse Size-Controlled Silver Decahedral Nanoparticles and Their Remarkable Optical Properties. *Chem. Mater.* **2008**, *20*, 5186−5190.
(22) Zhang, Q.; Yang, Y.; Li, J. R.; Iurilli, R.; Xie, S.; Qin, D. Citrate-Free Synthesis of Silver Nanoplates and the Mechanistic Study. *ACS Appl. Mater. Interfaces* **2013**, *5*, 6333−6345.
(23) Xia, X.; Zeng, J.; Zhang, Q.; Moran, C. M.; Xia, Y. Recent Developments in Shape-Controlled Synthesis of Silver Nanocrystals. *J. Phys. Chem. C* **2012**, *116*, 21647−21656.
(24) Xia, X.; Zeng, J.; Oetjen, L. K.; Li, Q.; Xia, Y. Quantitative Analysis of the Role Played by Poly(VinylPyrrolidone) in Seed-Mediated Growth of Ag Nanocrystals. *J. Am. Chem. Soc.* **2012**, *134*, 1793−1801.
(25) Zeng, J.; Zheng, Y.; Rycenga, M.; Tao, J.; Li, Z. Y.; Zhang, Q.; Zhu, Y.; Xia, Y. Controlling the Shapes of Silver Nanocrystals with Different Capping Agents. *J. Am. Chem. Soc.* **2010**, *132*, 8552−8553.
(26) Sun, X.; Qin, D. Co-Titration of $AgNO_3$ and $HAuCl_4$: A New Route to the Synthesis of Ag@Ag-Au Core-frame Nanocubes with Enhanced Plasmonic and Catalytic Properties. *J. Mater. Chem. C* **2015**, *3*, 11833−11841.
(27) Ahn, J.; Zhang, L.; Qin, D. Transforming Noble-Metal Nanocrystals into Complex Nanostructures through Facet-Selective Etching and Deposition. *ChemNanoMat* **2020**, *6*, 5−14.
(28) Ahn, J.; Wang, D.; Ding, Y.; Zhang, J.; Qin, D. Site-Selective Carving and Co-Deposition: Transformation of Ag Nanocubes into Cancaved Nanocrystals Encased by Ag-Au Alloy Frames. *ACS Nano* **2018**, *12*, 298−307.

(29) Zhou, S.; Li, J.; Gilroy, K. D.; Tao, J.; Zhu, C.; Yang, X.; Sun, X.; Xia, Y. Facile Synthesis of Silver Nanocubes with Sharp Corners and Edges in an Aqueous Solution. *ACS Nano* **2016**, *10*, 9861−9870.
(30) Ahn, J.; Kim, J.; Qin, D. Orthogonal Deposition of Au on Different Facets of Ag Cuboctahedra for the Fabrication of Nanoboxes with Complementary Surfaces. *Nanoscale* **2020**, *12*, 372−379.
(31) Zhang, L.; Zhang, Y.; Ahn, J.; Wang, X.; Qin, D. Defect-Assisted Deposition of Au on Ag for the Fabrication of Core-Shell Nanocubes with Outstanding Chemical and Thermal Stability. *Chem. Mater.* **2019**, *31*, 1057−1065.
(32) Zhang, Y.; Ahn, J.; Liu, J.; Qin, D. Syntheses, Plasmonic Properties, and Catalytic Applications of Ag-Rh Core-Frame Nanocubes and Rh Nanoboxes with Highly Porous Walls. *Chem. Mater.* **2018**, *30*, 2151−2159.
(33) Zhang, W.; Yang, J.; Lu, X. Tailoring Galvanic Replacement Reaction for the Preparation of Pt/Ag Bimetallic Hollow Nanostructures with Controlled Number of Voids. *ACS Nano* **2012**, *6*, 7397−7405.
(34) Luo, Z.; Ahn, J.; Qin, D. Fabrication of Ag−Pd concave nanocrystals through facet-selective oxidation of Ag atoms. *Nanoscale* **2019**, *11*, 6710−6718.
(35) Kettemann, F.; Wuithschick, M.; Caputo, G.; Kraehnert, R.; Pinna, N.; Rademann, K.; Polte, J. Reliable Palladium Nanoparticle Syntheses in Aqueous Solution: the Importance of Understanding Precursor Chemistry and Growth Mechanism. *CrystEngComm* **2015**, *17*, 1865−1870.
(36) Ducamp-Sanguesa, C.; Herrera-Urbina, R.; Figlarz, M. Synthesis and Characterization of Fine Monodisperse Silver Particles of Uniform Shape. *J. Solid State Chem.* **1992**, *100*, 272−280.
(37) Christopher, P.; Linic, S. Engineering Selectivity in Heterogeneous Catalysis: Ag Nanowires as Selective Ethylene Epoxidation Catalysts. *J. Am. Chem. Soc.* **2008**, *130*, 11264−11265.
(38) Li, Z.; Ji, S.; Liu, Y.; Cao, X.; Tian, S.; Chen, Y.; Niu, Z.; Li, Y. Well-Defined Materials for Heterogeneous Catalysis: From Nanoparticles to Isolated Single-Atom Sites. *Chem. Rev.* **2020**, *120*, 623−682.
(39) Tian, Z.-Q.; Ren, B.; Li, J.-F.; Yang, Z.-L. Expanding generality of Surface-Enhanced Raman Spectroscopy with Borrowing SERS Activity Strategy. *Chem. Commun.* **2007**, *34*, 3514−3534.
(40) Li, J.; Wu, Y.; Sun, X.; Liu, J.; Winget, S. A.; Qin, D. A Dual Catalyst with SERS Activity for Probing Stepwise Reduction and Oxidation Reactions. *ChemNanoMat* **2016**, *2*, 786−790.
(41) Nakatsuji, H.; Hada, M.; Yonezawa, T. Theoretical Study on the Chemisorption of a Hydrogen Molecule on Palladium. *J. Am. Chem. Soc.* **1987**, *109*, 1902−1912.
(42) Yu, W.; Mullen, G. M.; Mullin, C. B. Hydrogen Adsorption and Absorption with Pd−Au Bimetallic Surfaces. *J. Phys. Chem. C* **2013**, *117*, 19535−19543.
(43) Perera, G.; Ansar, S. M.; Hu, S.; Chen, M.; Zou, S.; Pittman, C. U.; Zhang, D. Ligand Desorption and Desulfurization on Silver Nanoparticles Using Sodium Borohydride in Water. *J. Phys. Chem. C* **2014**, *118*, 10509−10518.
(44) Shi, S.; Zhang, Y.; Ahn, J.; Qin, D. Revitalizing Silver Nanocrystals as a Redox Catalyst by Modifying Their Surface with an Isocyanide-Based Compound. *Chemical Science* **2020**, *11*, 11214−11223.
(45) Ahn, J.; Qin, D. Fabrication of Nanoscale Cage Cubes by Drilling Orthogonal, Intersected Holes through All Six Side Faces of Ag Nanocubes. *Chem. Mater.* **2019**, *31*, 9179−9187.
(46) Zhang, J.; Liu, J.; Xie, Z.-X.; Qin, D. $HAuCl_4$: A Dual Agent for Studying the Chloride-Assisted Vertical Growth of Citrate-Free Ag Nanoplates with Au Serving as a Marker. *Langmuir* **2014**, *30*, 15520−15530.
(47) Murshid, N.; Gourevich, I.; Coombs, N.; Kitaev, V. Gold Plating of Ag Nanoparticles for Superior Stability and Preserved Plasmonic and Sensing Properties. *Chem. Commun.* **2013**, *49*, 11355−11357.
(48) Zheng, H.; Smith, R. K.; Jun, Y.; Kisielowski, C.; Dahmen, U.; Alivisatos, A. P. Observation of Single Colloidal Platinum Nanocrystal Growth Trajectories,. *Science* **2009**, *324*, 1309−1312.
(49) Kwon, S. G.; Krylova, G.; Phillips, P. J.; Klie, R. F.; Chattopadhyay, S.; Shibata, T.; Bunel, E. E.; Liu, Y.; Prakapenka, V. B.; Lee, B.; Shevchenko, E. V. Heterogeneous Nucleation and Shape Transformation of Multicomponent Metallic Nanostructures,. *Nat. Mater.* **2015**, *14*, 215−223.
(50) Zhang, Y.; Liu, J.; Ahn, J.; Xiao, T.-H.; Li, Z.-Y.; Qin, D. Observing the Overgrowth of a Second Metal on Silver Cubic Seeds in Solution by Surface-Enhanced Raman Scattering. *ACS Nano* **2017**, *11*, 5080−5086.
(51) Wu, Y.; Qin, D. In Situ Atomic-Level Tracking of Heterogeneous Nucleation in Nanocrystal Growth with an Isocyanide Molecular Probe. *J. Am. Chem. Soc.* **2018**, *140*, 8340−8349.


https://doi.org/10.1021/accountsmr.1c00269
*Acc. Mater. Res.* 2022, 3, 391−402